Supplementary Information

Highly fluorescent scandium-tetracarboxylate framework: Selective detection of nitro-aromatic compounds, Sensing mechanism, and Its application

[a] *State Key Laboratory of Sensor Technology, and Institute of Solid State Physics, Hefei Institute of Physical Science, Chinese Academy of Sciences, Hefei, Anhui 230031, P. R. China.*

[b] *Institutes of Physical Science and Information Technology, Anhui University, Hefei, Anhui 230031, P. R. China.*

[c] *High Magnetic Field Laboratory, CAS Key Laboratory of High Magnetic Field and Ion Beam Physical Biology, Hefei Institutes of Physical Science, Chinese Academy of Sciences, Hefei, Anhui, 230031, P. R. China*

[d] *University of Science and Technology of China, Hefei, Anhui 230031, P. R. China.*

[e] *Key Laboratory of Environmental Optics and Technology, Anhui Institute of Optics and Fine Mechanics, Chinese Academy of Sciences, Hefei, Anhui 230031, P. R. China*

**Corresponding authors: Tel: +86 551 65595607; Fax: +86 551 65592420; E-mail: whxu@iim.ac.cn (W. Xu), junfeng@hmfl.ac.cn (J. Wang), zhiwuyu@hmfl.ac.cn (Z. Yu)*

Spectroscopy Study

The fluorescence spectra of **Sc-EBTC** crystals in various solvents and ligand H_4EBTC in DMF were recorded. 1 mg of fully ground **Sc-EBTC** crystals were dispersed (or 1 mg of H_4EBTC was dissolved) in 2.5 mL solvents. UV-vis absorption spectra were recorded with 0.8 mg of **Sc-EBTC** crystals (or H_4EBTC) in 3 mL DMF.

In the PL detection process, there are two main reasons for choosing DMF instead of water as the solvent. One reason is that the dispersion of **Sc-EBTC** in DMF is obviously better than that in water. **Sc-EBTC** is poorly dispersed in water, which might be due to its hydrophobic properties caused by hydrophobic channels.[1] **Sc-EBTC** not only has good dispersion but also excellent fluorescence characteristics in DMF, moreover, it has been widely observed in the previous study that usually use DMF as solvent to detect NACs.[2-4] For example, $[Zn_4(BPTC)_2(NMP)_3(DMF)(H_2O)_2]_n$ (BPTC= biphenyl-3,3′,5,5′-tetracarboxylic acid, NMP= N-methyl pyrrolidone) dispersed in DMF to detect 2,4-DNT, 1,3-DNB and PNP,[2] and $[Zn_2(TPOM)(NH_2–BDC)_2]\cdot 4H_2O$ (TPOM =tetrakis (4-pyridyloxymethylene)methane, NH_2–BDC=2-aminoterephthalic acid) dispersed in DMF to detect 4-NP,[3] and so on. Another reason is that the detection effect of **Sc-EBTC** in DMF is better than its effect in water. Taking the detection of 2,4-DNP (0-138 μM) as an example, as shown in Fig. S8, the quenching constants K_{sv} of **Sc-EBTC** in DMF is 2.85×10^4 M^{-1} (max. quenching efficiency is about 85%), and its quenching constant Ksv in water is 2.30×10^4 M^{-1}(max. quenching efficiency is about 77%).

Activation of Sc-EBTC

The 100 mg **Sc-EBTC** crystals were ground thoroughly and soaked in 10 mL DMF for 48 hours, and the fresh DMF solution was replaced every 8 hours. Then, the **Sc-EBTC** was soaked in the 10 mL THF solution for 48 hours in the same procedure. Finally, it was centrifuged and dried in a vacuum drying oven at 80°C for 48 hours to obtain the activated **Sc-EBTC**.

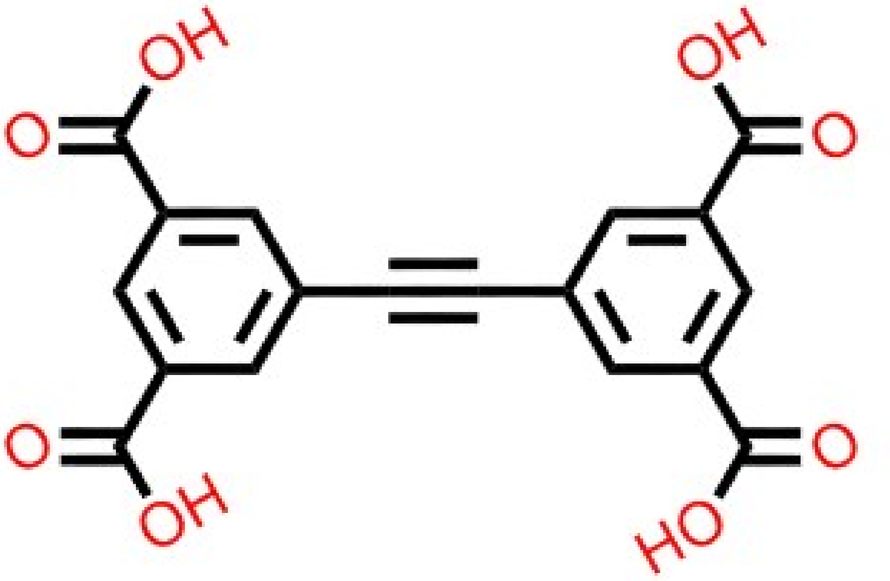

Fig. S1 Illustration for the Molecular Structure of H_4EBTC.

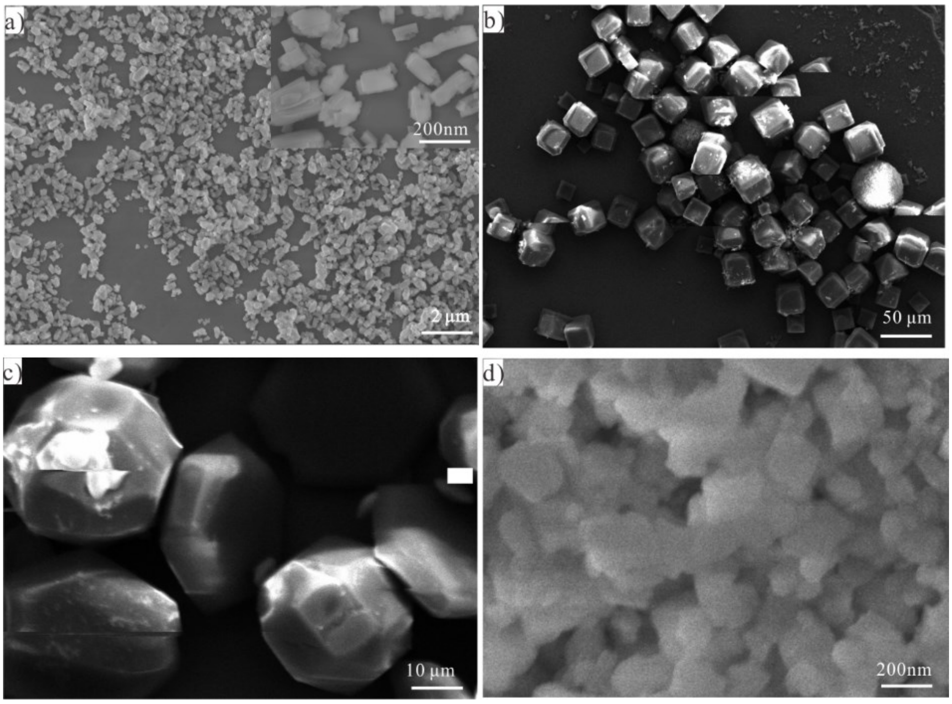

Fig. S2 SEM images of **Sc-EBTC** crystals. The crystal morphological of **Sc-EBTC** would evolve from simple cubes to complex octadecahedra with increasing amount of acetic acid during the synthesis. a) nanosheets (0 µL acetic acid), b) cube (about 5 µL acetic acid), c) octadecahedra (about 7.5 µL acetic acid). d) SEM images of **Sc-EBTC** after grinding.

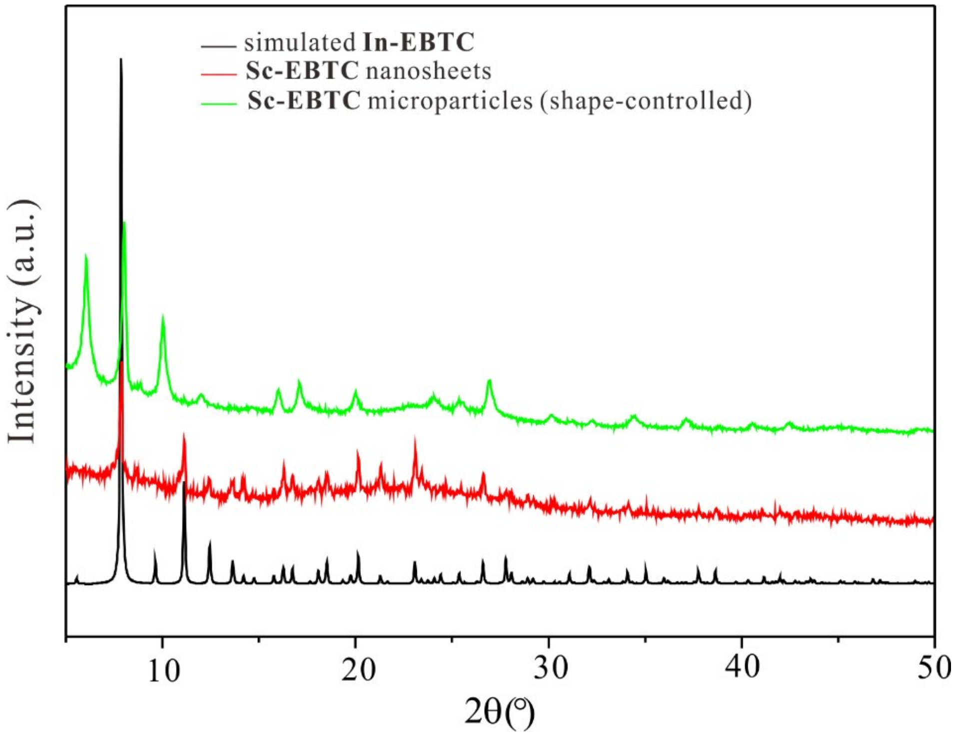

Fig. S3 PXRD patterns of synthesized **Sc-EBTC** crystals. **Sc-EBTC** nanosheets (green), shape-controlled **Sc-EBTC** microparticles (red), and simulated by **In-EBTC** (black).

The diffraction peaks of shape-controlled **Sc-EBTC** crystals correspond well with simulated by **In-EBTC**, indicating the pure phase of **Sc-EBTC**. Whereas, broadened and weakened reflections of **Sc-EBTC** sheets were attributed to excessively small crystallite size.[1]

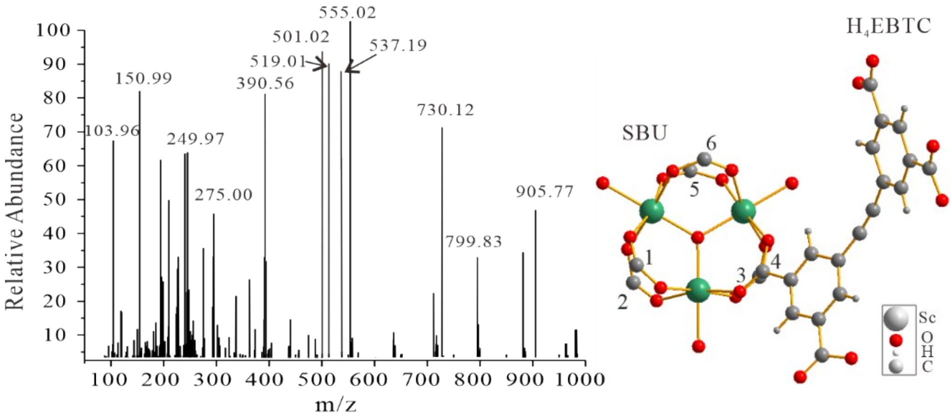

Fig. S4 Mass spectra of **Sc-EBTC**.

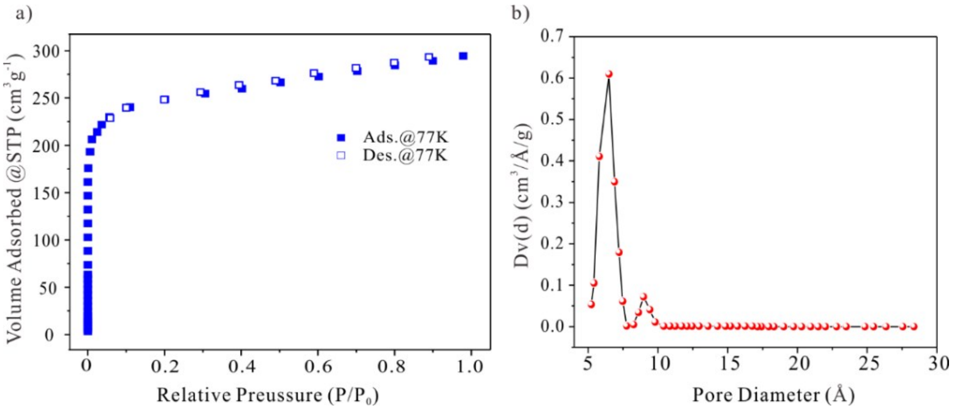

Fig. S5 N_2 gas adsorption isotherms and pore size distribution analysis for **Sc-EBTC**.

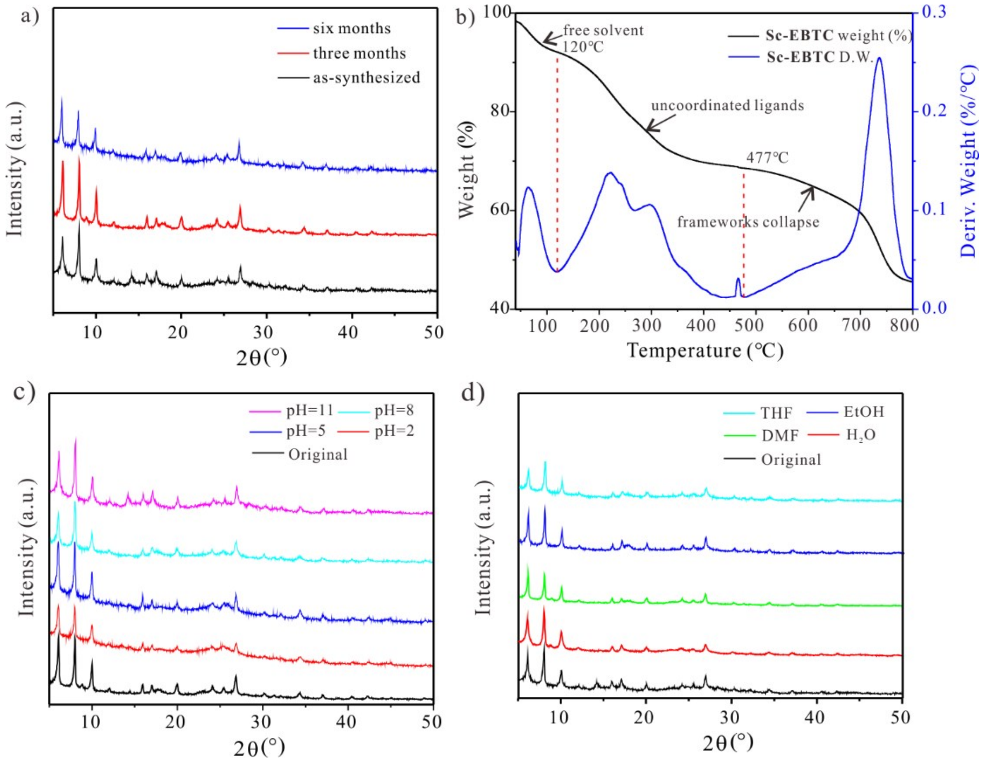

Fig. S6 Stability of **Sc-EBTC**. The PXRD patterns of **Sc-EBTC,** a) sealed in test tube for 3 months and 6 months, and immersed in c) various solvent and d) different pH solution for 24 hours; b) TG curve (black) and the weight derivative curve (blue) of **Sc-EBTC** in nitrogen condition.

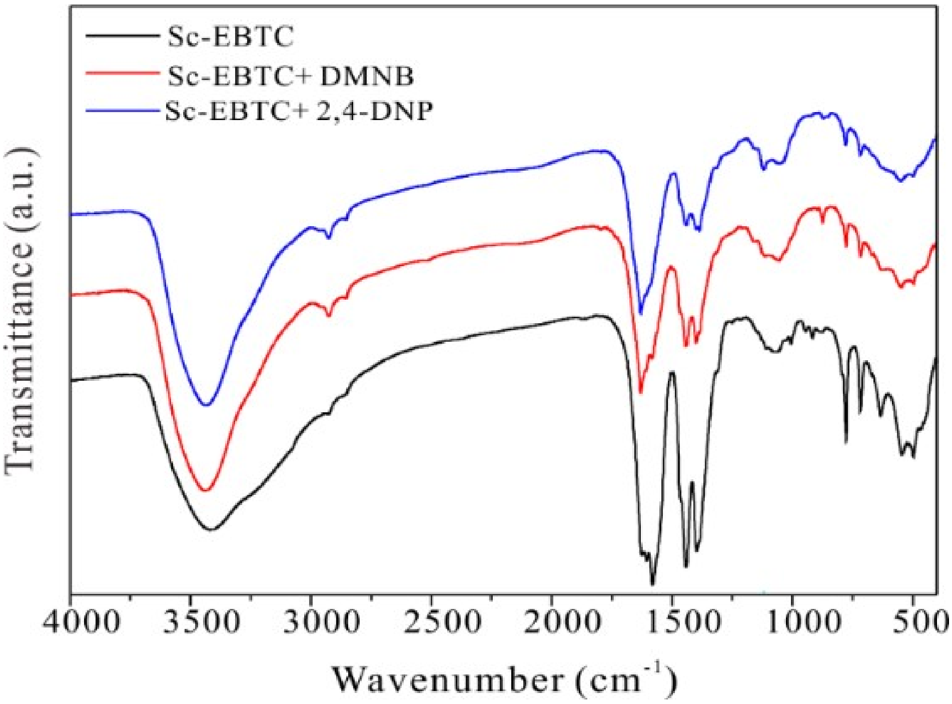

Fig. S7 FT-IR spectra of pristine **Sc-EBTC** (black) and **Sc-EBTC** immersed in DMNB (red) and 2,4-DNP (blue).

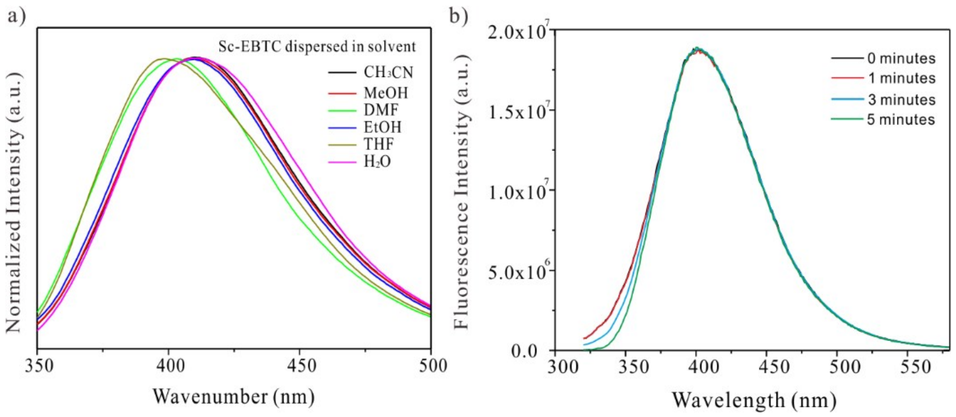

Fig. S8 a) Normalized fluorescence spectra of **Sc-EBTC** dispersed in different solvents. b) Fluorescence spectra of ground **Sc-EBTC** dispersed in DMF after standing for few minutes (standing time = 0, 1, 3, 5 minutes). (λ_{ex} 300 nm, slit widths 2.0 nm for excitation and emission, respectively.)

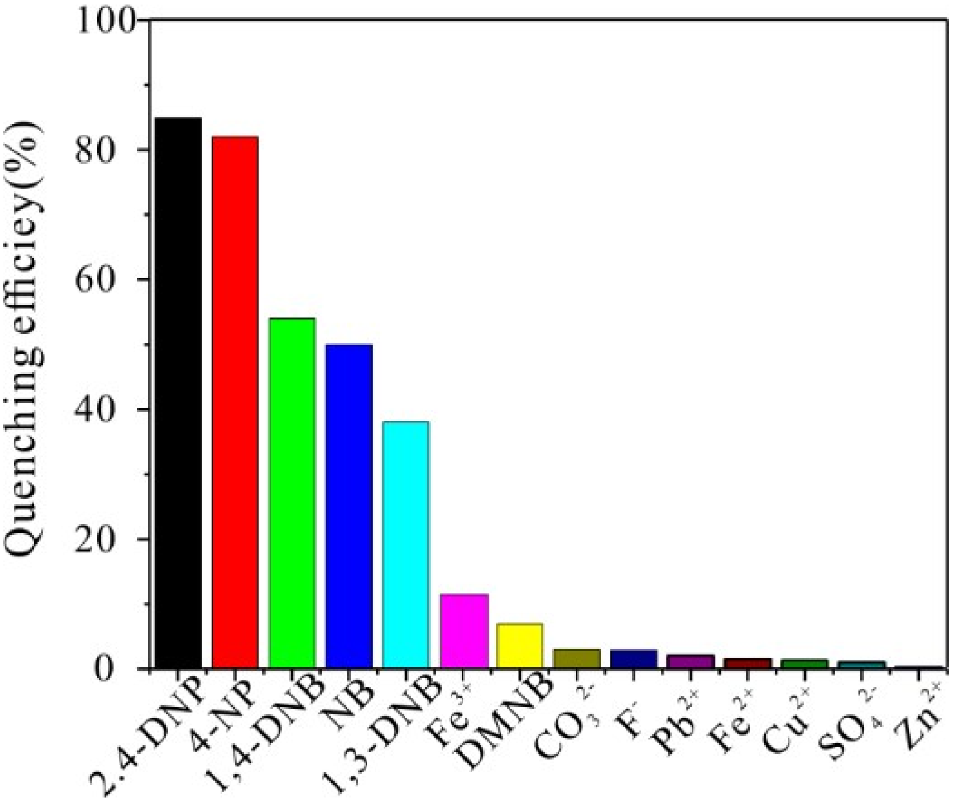

Fig. S9 Fluorescence quenching experiments of selective detection for NACs. The concentrations of **Sc-EBTC** DMF suspension and the analytes are 0.4 mg/mL and 138 μM, respectively.

To examine the selective sensing abilities of **Sc-EBTC** toward NACs, the different analytes (138 μM) including 2,4-DNP, 4-NP, 1,4-DNB, 1,3-DNB, NB, DMNB, and ions (F^-, SO_4^{2-}, Fe^{3+}, Fe^{2+}, Pb^{2+}, Cu^{2+}, Zn^{2+}) were added into **Sc-EBTC** suspension, respectively, and after the mixture was shaken for 30 seconds, the fluorescence was measured immediately at room temperature. As shown in **Fig. S11**, the fluorescence of **Sc-EBTC** after adding DMNB was hardly changed, while the NACs (such as 2,4-DNP and 4-NP) significantly quenched the fluorescence, indicating that **Sc-EBTC** was more selective in the detection of NACs than the other analytes.

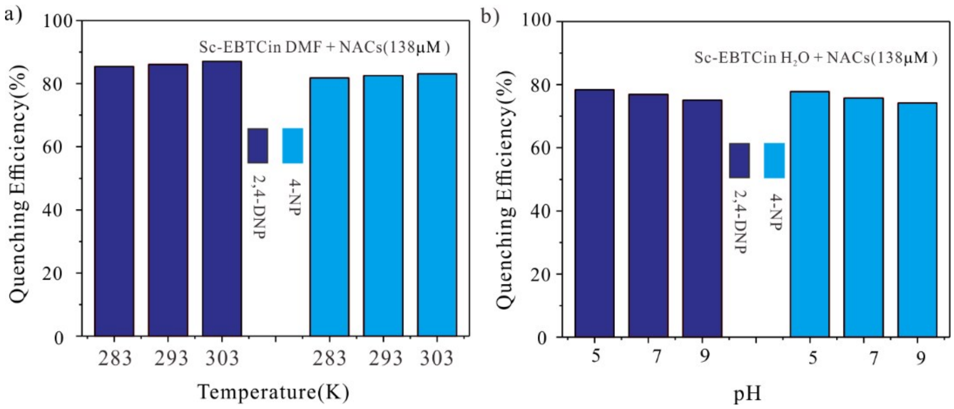

Fig. S10 Effect of a) temperature and b) pH value on the quenching of fluorescent **Sc-EBTC** by 2,4-DNP and 4-NP.

We further explored the effect of temperature and pH. As shown in Fig. S10, the quenching efficiency of **Sc-EBTC** DMF suspension by 2,4-DNP/4-NP (138 μM) at about 283K, 293K and 303K was 85.4%/81.8%, 86.1%/82.5% and 87.1%/83.2%, respectively, which indicates that temperature has little influence on the detection of NACs by **Sc-EBTC**. And the quenching efficiency of **Sc-EBTC** H_2O suspension by 2,4-DNP/4-NP (138 μM) at pH=5, 7 and 9 was 79.8%/78.7%, 77.6%/76.2%, and 76.5%/75,4%, respectively, which indicates that pH has little influence on the detection of NACs by **Sc-EBTC** as well.

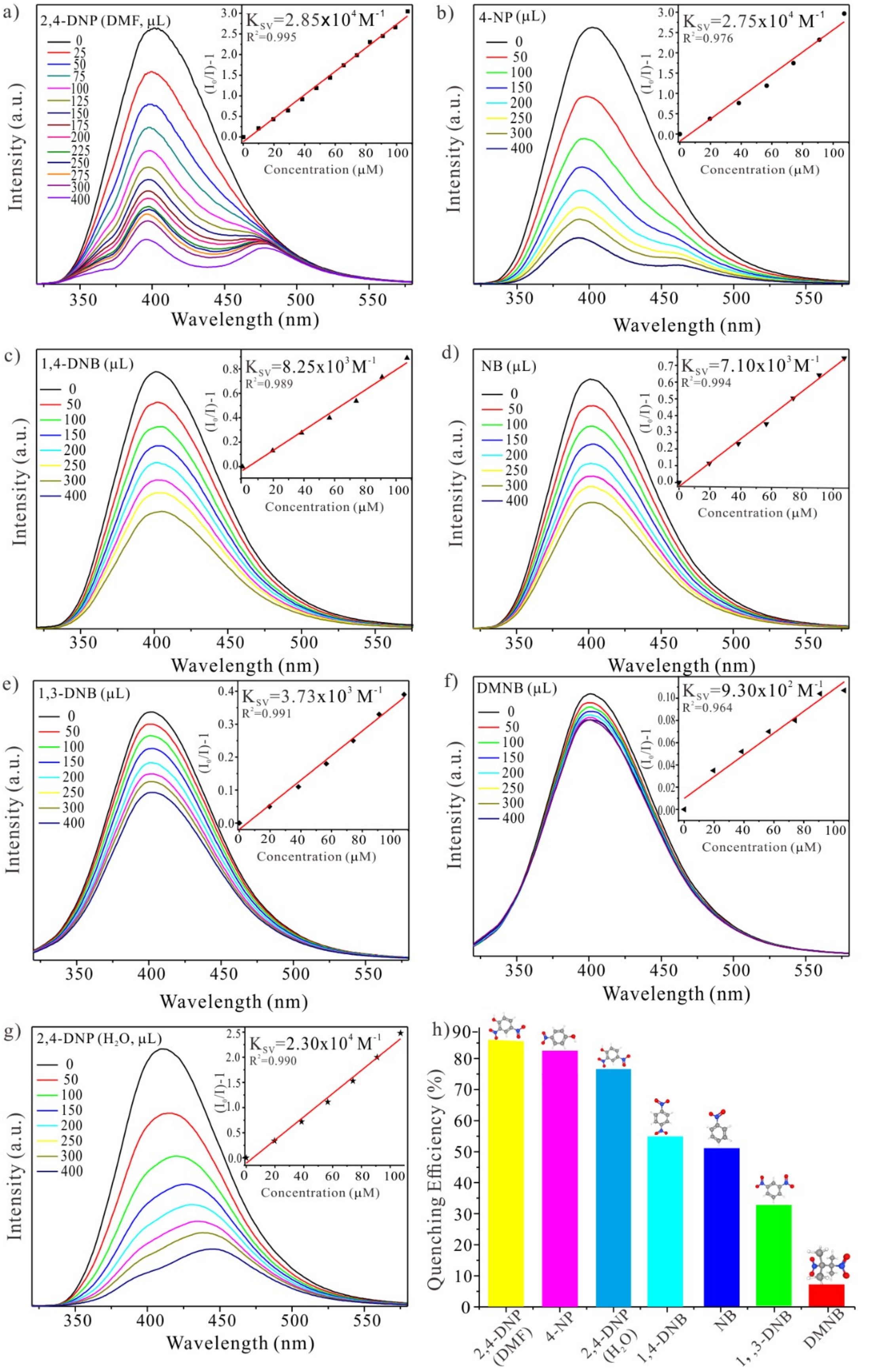

Fig. S11 Concentration-dependent (0-138 μM) fluorescence intensities of **Sc-EBTC**

suspension by the addition of different volumes of 1 mM of analytes: a) 2,4-DNP (DMF), b) 4-NP, c) 1,4-DNB, d) NB, e) 1,3-DNB, f) DMNB, and g) 2,4-DNB (H_2O). h) The percentage of fluorescence quenching of **Sc-EBTC** suspension in the presence of different the analytes (138 μM) at RT. The inserts are S-V plots. Note: a-f) **Sc-EBTC** dispersed in DMF; g) **Sc-EBTC** dispersed in H_2O. (λ_{ex}=300 nm, slit width 2.0 nm)

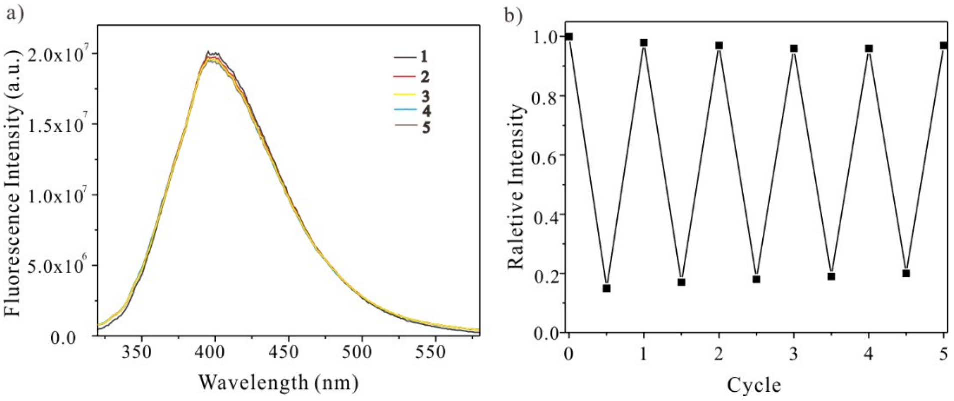

Fig. S12 Recyclability of **Sc-EBTC** observed over 5 cycle.

To further verify the stability of material testing, **Sc-EBTC** was recycled 5 times to detect 2,4-DNP (138 μM), the results were shown in Fig. S12. The quenching efficiency of **Sc-EBTC** toward 2,4-DNP was still over 80% in the fifth test, and its fluorescence could still return to the initial state after simple ultrasonic cleaning with DMF, as shown in Fig. S12. This shows that **Sc-EBTC** has practical application potential in practice.

Detection Limit for 2,4-DNP and 4-NP with **Sc-EBTC** in DMF

For 2,4-DNP:

Detection Limit = 3σ/slope

= 3 * 2.41E4/2.30E6

= 0.031 μM

For 4-NP:

Detection Limit = 3σ/slope

= 3 * 2.41E4/1.60E6

= 0.045 μM

Multiple number of PL spectra (n = 11) were recorded for the Blank sample of **Sc-EBTC** suspension. Sample Standard Deviation σ for the blank probe, without the addition of NACs was calculated to be 2.41E6.

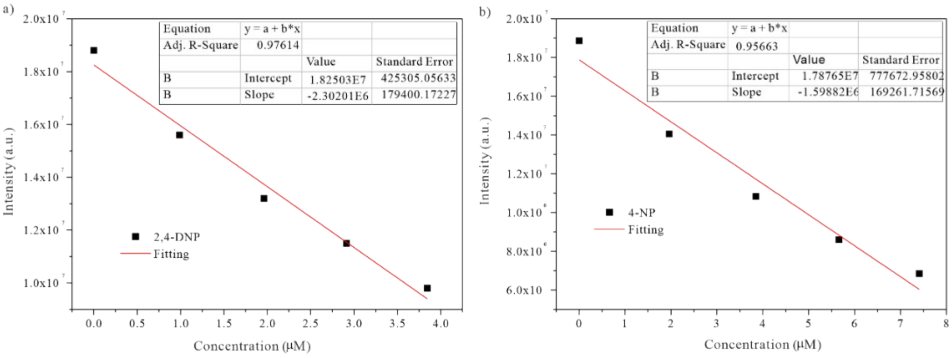

Fig. S13 Relation of fluorescence intensity against a) 2,4-DNP and b) 4-NP added into **Sc-EBTC** suspension and their linear fit curves for the estimation of detection limit.

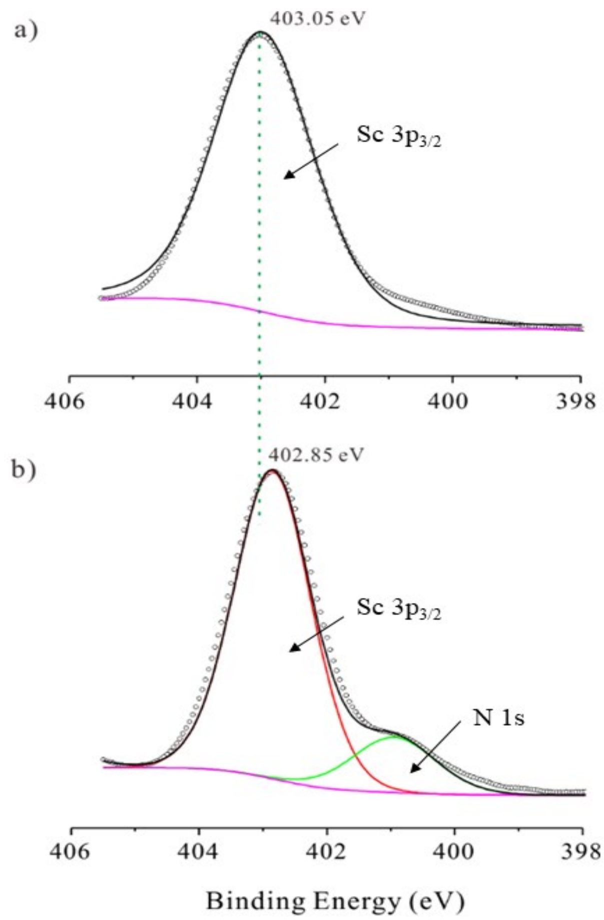

Fig. S14 X-ray photoelectron spectroscopy (XPS) of Sc $3p_{3/2}$: a) as-synthesized **Sc-EBTC**, b) **Sc-EBTC** immersed in 2,4-DNP solutions (0.1 mM) and then dried treatment.

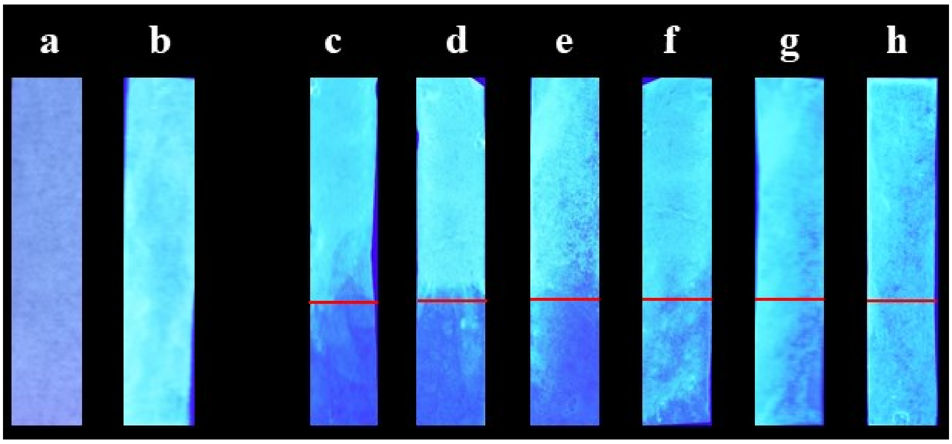

Fig. S15 Photo images of the test strips under 300 nm UV light and the interface in contact with the dilute solution of the analyte is indicated by a red line. Images of (a) blank test strip and (b) MOF @ test strip under 300 nm UV light. Images of MOF @ test strips bedewed with (c) 2,4-DNP (0.2 mM), (d) 4-NP (0.2 mM), (e) p-DNB (0.5 mM), (f) NB (0.5 mM), (g) m-DNB (0.5 mM), and (h) DMNB (1.0 mM).

Table S1. List of LMOFs sensors for aqueous-phase detection of 2,4-DNP

No.	LMOFs	K_{sv} (M^{-1})	Detection limits	Ref.
1	$\{[Zn_2(MTAIA)(DMF)_2(H_2O)]\cdot H_2O\}_n$	1.65×10^4	-	5
2	$\{(NH_2(CH_3)_2)[Zn_4(ddn)_2(COO)(H_2O)_4]\cdot solvent\}_n$	0.89×10^4	1.12 ppm	6
3	$\{[PbNa(TZBPDC)](H_2O)(DMF)_2\}_n$	1.25×10^4	0.88 ppm	7
4	$\{[Cd_2(tdz)_2(4,4'\text{-}bpy)_2]\cdot 6.5H_2O\}_n$	2.48×10^4	-	8
5	$[Cd(ppvppa)(1,4\text{-}NDC)]_n$	118	-	9
6	$[Zn_2(TCPE)(tta)_2]\cdot 2DMF\cdot 4H_2O\cdot 2Me_2NH_2^+$	2.60×10^4	7.83 ppb	10
7	**Sc-EBTC**	2.85×10^4	5.71 ppb	This work

Table S2. List of LMOFs sensors for aqueous-phase detection of 4-NP

No.	LMOFs	K_{sv} (M^{-1})	Detection limits	Ref.
1	$\{[Zn_2(MTAIA)(DMF)_2(H_2O)]\cdot H_2O\}_n$	1.03×10^4	-	5
2	$\{[Cd_2(tdz)_2(4,4'\text{-}bpy)_2]\cdot 6.5H_2O\}_n$	1.55×10^4	-	8
3	$[Cd(ppvppa)(1,4\text{-}NDC)]_n$	15	-	9
4	$[Zn_2(TCPE)(tta)_2]\cdot 2DMF\cdot 4H_2O\cdot 2Me_2NH_2$	0.16×10^4	94.59 ppb	10
5	(Eu-CP)$\{[Eu(L^1)(HCOO)]\cdot H_2O\}_n$	1.38×10^4	-	11
6	$[Tb_2(H_2L^2)_3(H_2O)_2]\cdot 21H_2O$	0.46×10^4	-	12
7	$[Cd(L^3)(IPA)]_n$	1.86×10^4	-	13
8	$[Zn(L^4)(H_2O)]\cdot H_2O$	1.25×10^4	0.52 ppm	14
9	$[Tb(BTEC)_{0.5}(HCOO)(H_2O)_2]$	2.04×10^4	-	15
10	$[(CH_3)_2NH_2][In(TNB)_{4/3}]\cdot(2DMF)(3H_2O)\supset DSM$	1.23×10^4	-	16
11	**Sc-EBTC**	2.75×10^4	6.26 ppb	This work

L^1 = 5-((pyridin-3-yloxy) methyl) isophthalic acid

L^2 = 1,4-$C_6H_4(CH(OH)(PO_3H_2))_2$

L^3 = 3-pyridin-3-yl-N-[5-(3-pyridin-3-yl-acryloylamino)-naphthalen-1-yl]-acrylamide

L^4 = 5-(2-methylpyridin-4-yl) isophthalic acid

DSM = 4-[p-(dimethylamino) styryl] 1-ethylpyridinium

Notes and References

1 A. Schaate, P. Roy, A. Godt, J. Lippke, F. Waltz, M. Wiebcke, and P. Behrens, *Chem. Eur. J.*, 2011, **17**, 6643-6651.

2 F. L. Fu, D. D. Dionysiou and H. Liu, *J. Hazard. Mater.*, 2014, **267**, 194-205.

3 P. Kovacic, and R. Somanathan, *J. Appl. Toxicol.*, 2014, **34**, DOI: 10.1002/jat.2980.

4 Y. Zhang, X. X. Ma, S. C. Zhang, C. D. Yang, Z. Ouyang, and X. R. Zhang, *Analyst.*, 2009, **134**, 176-181.

5 P. Das and S. K. Mandal, *J. Mater. Chem. A*, 2018, **6**, 21274-21279.

6 A. Ma, J. Wu, Y. Han, F. Chen, B. Li, S. Cai, H. Huang, A. Singh, A. Kumar, and J. Liu, *Dalton Trans.*, 2018, **47**, 9627-9633.

7 X. R. Wu, X. Shen, S. R. Fan, M. Trivedi, B. H. Li, A. Kumar, and J. Q. Liu, *RSC Adv.*, 2018, **8**, 23529-23538.

8 A. Gogia, and S. K. Mandal, *Dalton Trans.*, 2019, **48**, 2388-2398.

9 M. M. Chen, X. Zhou, H. X. Li, X. X. Yang, and J. P. Lang, *Cryst. Growth Des.*, 2015, **15**, 2753-2760.

10 X. D. Zhang, G. J. Ren, M. L. Li, W. T. Yang, and Q. H. Pan, *Cryst. Growth Des.*, 2019, **19**, 6308-6314.

11 Y. Liu, J. Ma, C. Xu, Y. Yang, M. Xia, H. Jiang, and W. Liu, *Dalton Trans.*, 2018, **47**, 13543-13549.

12 R. B. Fu, S. M. Hu, and X. T. Wu, *J. Mater. Chem. A*, 2017, **5**, 1952-1956.

13 D. Das and B. Kumar, *Cryst. Growth Des.*, 2018, **18**, 3683-3692.

14 X. Y. Guo, F. Zhao, J. J. Liu, Z. L. Liu, and Y. Q. Wang, *J. Mater. Chem. A*, 2017, **5**, 20035-20043.

15 R. F. Bogale, Y. Z. Chen, J. W. Ye, Y. Y. Yang, A. Rauf, L. Y. Duan, P. Tian, and G. L. Ning, *Sens. Actuators B Chem.*, 2017, **245**, 171-178.

16 H. R. Fu, Y. Zhao, T. Xie, M. L. Han, L. F. Ma, and S .Q. Zang, *J. Mater. Chem. C*, 2018, **6**, 6440-6448.